LAWRENCE
LIVERMORE
NATIONAL
LABORATORY

LLNL-JRNL-489847

Evaporation kinetics of laser heated silica in reactive and inert gases based on near-equilibrium dynamics

S. Elhadj, M. J. Matthews, S. T. Yang, D. Cooke

June 29, 2011

Optics Express

Disclaimer

Evaporation kinetics of laser heated silica in reactive and inert gases based on near-equilibrium dynamics

S. Elhadj*, M.J. Matthews, S. T. Yang, D. Cooke

Lawrence Livermore National Laboratory, 7000 East Avenue, L-491, Livermore, CA 94550-9234, USA
*Corresponding author Tel.: 925 422 0270; Fax 925 422 2041. E-mail address: elhadj2@llnl.gov

ABSTRACT

The temperature dependent evaporation kinetics of silica was measured up to the boiling point~3000 K using a CO_2 laser for heating, while the solid-gas phase evaporation chemistry of silica was assessed by using, hydrogen, air, and pure nitrogen gases that served to represent reducing, oxidizing, and neutral environments, respectively. Air, nitrogen, and hydrogen were increasingly more effective in evaporating silica at a given temperature in that order. Hydrogen gas enhancement was attributed to providing an additional pathway for the formation of the evaporation product SiO, while the oxygen in air pushed the balance of the reaction backwards. The problem of mass transport control was addressed experimentally with a gas-nozzle flow configuration co-aligned with the infrared laser heating that allowed varying the gas species feed and removal rates. The apparent mass transport limitations supported the use of a near-equilibrium analysis for the purposes of interpreting the evaporation kinetic data. In combination with an evaporation reaction schemes provided for each gas, the thermodynamics of the reactions were determined and the effective reaction free energies were derived from 2600 K to 3000 K and compared to reported values. With the corresponding mass transfer coefficient, a semi-empirical model of the evaporation kinetics of silica is derived that accounts for the heating, gas chemistry, and transport parameters. The experimental and analytical approach described should have broad application to material evaporation, but also in applications requiring study of thermal decomposition chemistry under extreme temperatures.

Research highlights

- Evaporation rates of laser heated fused silica were measured from 2600-3000 K in the presence of hydrogen, air, and pure nitrogen gases
- The solid-gas phase chemistry of the reactions involved with oxidizing, neutral, and reducing gases were determined
- The process of silica evaporation was found to be mass transport limited
- A near equilibrium model is derived to describe the evaporation of silica based on temperature, gas composition, and gas flow rate

Keywords:

Silica, laser, infrared, gas, reducing, hydrogen, oxygen, nitrogen, evaporation rate, flow, temperature, mass transfer coefficient, equilibrium

1. Introduction

Silica plays a critical role in many industrial applications such as raw material in refractory linings, fiber optics, optical substrates and, in general, as a component in devices requiring inertness and toughness. However, the same properties that make silica attractive also make it difficult to process. High temperatures above the glass working point (~2400 K) are required for molding of fused silica, while very reactive species are needed for its chemical etching [1, 2]. Furthermore, many of its processing properties depend exponentially on temperature [3-7]. In particular, silica evaporative etching requires extreme temperatures approaching its boiling point of ~3000K [8] to be practical for machining under ambient conditions [9-11]. In applications where localized heating is used for machining glass in air these high temperature requirements are often associated with unwanted increases in residual stresses [12], formation of rim structures [10, 13], and redeposit defects [11]. A reduction in the treatment temperature required for material removal would therefore improve thermal processing in general since the material changes involved are common to a broad range of materials. One approach, which is evaluated in this study, is to reduce the laser-driven vapor pressure of silica through the implementation of reactive gases in a flow configuration to assist evaporation.

Although the kinetics of a broad range of solid-gas phase chemistry on the evaporation of silica have been studied [8, 14-20], systematic studies near the boiling point of silica are lacking because most containment vessels degrade above ~2000K [21]. Moreover, *in situ* measurements become blurred from both high blackbody radiation background and high fluxes. In this work, laser heating was used as a means to reach surface temperatures up to 3000 K at the gas –solid interface, and the impact of selected gas reactivities on the evaporation kinetics of silica could thus be readily assessed at high temperatures. To determine the effect of a broad range of functional chemistries, air, hydrogen-nitrogen mixture, and pure nitrogen gases were selected to relate evaporation kinetics to an oxidizing, reducing, and inert atmosphere, respectively. For these chemistries, the dependence of the evaporation kinetics on temperature and gas flow rate were derived from measurements of the surface temperature and shape profiles of the silica pits formed when exposed to continuous laser heating and controlled gas flow.

Classical treatments of laser-based evaporation model evaporation kinetics based on the velocity distribution of escaped species within the Knudsen layer close to a hot surface [22]. However, this type of analysis does not account for the specific chemical reactions that occur from a reacting gas, or any shift in the equilibrium of the evaporation reactions from the presence of a gas phase product. In addition, the impact of convective transport resulting from the net evolution of gas products at the reacting surface [23] or from forced convection is similarly not accounted for by the Knudsen layer modeling. Here we implement for the first time an analysis for laser-based evaporation that assumes near-equilibrium conditions [24] within a boundary layer where most of the variation in the species concentration occurs. The equilibrium concentration in the vicinity of the gas-solid interface establishes the driving force for the rate of diffusive transport within the boundary layer before mixing and removal in the bulk of the gas stream. The boundary layer thickness, in turn, depends on the gas properties, flow rate, and flow configuration, and determines the transport kinetics via the mass transport coefficient,

$h_m \sim D/\delta$ where D is the gas species diffusivity and δ is the boundary layer thickness. Therefore, a predictive model is presented for laser-based evaporation obtained through determination of the h_m and equilibrium constants, K_p, from which equilibrium concentrations are calculated. The analysis of the evaporation rate data described here provides a means to probe the role of chemical reaction thermodynamics and transport kinetics at the extreme temperatures reached during laser heating of materials in general.

2. Experimental approach and details

2.0. Experimental approach

A schematic of the laser and setup used to heat and apply gas to the surface of the fused silica sample is shown in Fig. 1A. Figure 1B illustrates representative measurements of the pit depth and surface temperature profile used to derive the temperature-dependent evaporation rates resulting from silica laser heating. Temperature measurements were obtained from infrared imaging of the blackbody radiation emitted during heating. The amount of evaporated silica was estimated from the surface shape profiles obtained by interferometry measurements following treatment of the surface. Finally, gas flow rate levels were adjusted with a flow controller, directing a normal incidence gas jet towards the sample surface through a custom nozzle equipped with a laser window for simultaneous laser heating. Additional details of the measurements and setup are provided below.

2.1. Heating of silica surface

Localized heating and evaporation of the silica surface was achieved with a focused CW (λ_L = 10.6 μm) CO_2 laser beam from a Synrad Firestar V20 (Synrad, Mukilteo, WA, USA), with a maximum output power of 20W and power stability of ~1% over the duration of the exposure. The laser beam profile was nearly a perfect Gaussian with a $1/e^2$ diameter of ~1 mm, as characterized by a beam profiler (Pyrocam III, Spiricon). The laser power delivered to the sample was set between 6.5 and 7.2W, while the exposure time was fixed at 5 s. A far infrared laser was selected because laser energy couples efficiently to a narrow absorption depth of~3-40 μm at λ_L [7], thus surface temperatures in excess of 3000K could readily be achieved. However, evaporation above 3000K produced deeper pits that became more difficult to resolve to get surface profile by interferometry. In addition, the Fresnel reflectivity, and hence net laser absorption, tends to decrease when the aspect ratio of the pit (depth to width) approaches ~1. In contrast, temperatures between 2100 and 2500 K produced shallower pits for which the effects on pit depth from the thermally-induced densification of silica [4] became significant. The resulting surface depressions – distinguishable from those of due to evaporation - were as deep as 100 nm, or about 10% or more of the total pit depth. Below 2100 K, owing to the exponential dependence of the evaporation on temperature, pit depth was dominated by silica compaction such that contributions due to evaporation could not be determined. For these reasons, the exposure time and range of temperatures in this study were optimized as stated to effectively study silica evaporation around its boiling point (2500 – 3100 K).

2.2. Gas treatment of the silica surface

The samples used in this study were Corning 7980 (type III) fused silica (50 mm diameter, 10 mm thick discs). They were fixed vertically on a stage in ambient air and treated by injecting reactive gases using a nozzle with a 3 mm opening in front. Sample-surface spacing was kept fixed ~5 mm. The gas jet impinged normal to the surface plane and submerged the treated area well beyond the boundaries of the heated site by displacing the ambient air at the reacting surface before onset of laser heating. The laser beam passes through a transparent ZnSe window mounted on the backside of the nozzle and on to the surface through the nozzle front side opening. Compressed gas cylinders were used as the source for the following four dry gases (<1 ppmv H_2O), with trace amounts of impurities (< 3 ppmv): 1) dry air (78% nitrogen, 21% oxygen, 1% trace gases), 2) 100% nitrogen, 3) 5% hydrogen, 95% nitrogen, 4) 5% hydrogen, 95% helium. A calibrated OMEGA gas flow controller (FMA 3400) allowed setting the volumetric flow rate to levels up to ~10L/min. The flow was started at least a minute before laser exposure to insure that all the dead volume was removed from the lines and that surface gas submersion was at steady state.

2.3. Depth profile measurement of the silica surface

As discussed in the Results and Discussion section, the amount of material removed at the center of the laser created pits can be attributed exclusively to the net amount of evaporated material. Therefore, after laser exposure, the surface profiles were measured using a ZYGO white light interferometer (Zygo Corp., Middlefield, CT, USA) to determine the pit depth and thus the amounts of evaporated silica at the laser heated sites. The vertical resolution of the instrument is on the order of 1 nm and the lateral resolution ~ 0.5 μm. Measured maximum depths at the center of the pits ranged from 1 to 45 μm; and pit diameters ranged from 200 to 500 μm depending on the peak temperature and gas used.

2.4. Temperature measurement of silica surface

During laser exposure, the sample surface temperature was derived from *in situ* measurements of the blackbody emission from the heated spot using a calibrated LN-cooled HgCdTe camera operating at 33 fps and equipped with a λ_p=8.9 μm narrowbandpass cold filter [25]. Although the optical resolution of the camera was ~100 μm (sampled at 40 μm spacing), it can be shown that the calculated temperature profile established by a 1 mm beam varies quite slowly over the length scales studied here. Thermal imaging in a narrow band in the far infrared (λ_p) is crucial because it probes the surface emission exclusively within ~1 μm of the outer surface of silica, which results in an accurate temperature measurement of the interface rather than a bulk average over a gradient [26]. For the purposes of analyzing the data, the gas at the gas-solid interface was assumed to be rapidly thermalized to the measured temperature of the silica surface. For further details, the 2D surface temperature measurement method used in this study was validated and described elsewhere [25-27].

Results and Discussion

3.0 Estimate of the evaporation rates from surface profile

The temperature and composition dependent evaporation rate, $R(T, C_i)$, was estimated based on the measurement of the depth profile (Fig. 1B) as it relates to the amount of material removed by evaporation. The accuracy of this approach to derive R depends on the assumption that the depth at a particular location is the result of only the evaporation process, and not the result of flow of molten silica or material expulsion from explosive boiling [28]. At the center of the pit where the pit depth is maximum, that assumption is appropriate for two reasons. First, an estimate of the thermocapillary flow suggests relatively little contribution of flow-displaced silica to the total depth. The flow velocity, v_f, normal to the surface of the thermocapillary flow can be roughly approximated by $v_f=(d\gamma/dT)\Delta T/\mu$ [29], where $d\gamma/dT$ represents the rate of change of the surface tension with temperature, ΔT, is the temperature drop from the center of the pit to the edge of the pit (Fig. 1B), and μ is the dynamic viscosity. A plot of the flow induced displacement of silica in the pit versus peak temperature (see Supplementary section) shows that the thermocapillary flow contribution is expected to be no more than 2% of the total pit depth.

In addition, any material removed from drag associated with the gas feed flow should be negligible given the gases relative lack of inertia at atmospheric pressure, and the small superficial velocities involved in this study (<25 m/s). Contributions of vapor-induced shear forces and recoil pressure in shaping laser produced cavities in solids were shown to have a negligible impact on the cavity axial depth produced for the relatively slow evaporation conditions used in this study [30]. Finally, none of the surface profiles displayed any roughening within the pit that would normally occur if explosive boiling had taken place, and experimental irradiances were well below the phase explosion threshold (10^{11} W/cm^2) [28]. Therefore, in attributing the axial depth, d, solely to the evaporation of material at that location it is possible to derive a measure of the temperature dependent evaporation kinetics given by $R(T_p)\sim\rho\times d/\Delta t$, where $\sim\rho$ is the fused silica density, Δt is the laser exposure time, and T_p is the peak temperature measured at the center of the pit (Fig. 1B). Using the center depth is particularly convenient because the location of that spot can easily be found from the surface and temperature spatial profiles. Furthermore, restricting the analysis to that location circumvents any ambiguity arising from the non-uniform heating of the Gaussian-shaped laser beam. Finally, for the purposes of calculating evaporation rates, the effective exposure time was taken as Δt=4sec instead of the fixed experimental exposure of five seconds, since the thermal diffusion time needed to approach peak temperatures with thermal diffusivity D=8×10^{-7} m^2/s [25] is $\sim a^2/D$=0.98 sec, where a is the beam diameter. The resulting error based on the time-integrated experimental evaporation rates extrapolated to lower temperatures is expected to represent <3 % of the bottom pit depth.

3.1 Role of kinetics and rate controlling parameters

The analysis of the evaporation rate data depends on whether the process is transport limited or under reaction kinetics control. In the transport limited regime the controlling parameters are the mass transfer coefficient (h_m) and the reaction equilibrium constant (K_p) [24]. When transport is not limiting,

the rate constants for the evaporation and condensation reactions become the controlling parameters. The measurement of the *R* dependence on gas flow rate is used to distinguish between these two alternatives. A lack of dependence of *R* on flow rate would indicate that the process of evaporation is not transport limited. In Fig. 2, a representative measurement at 2880K indicates that there is a weak, but significant, dependence of the *R* on flow for all gases used. This was observed through the experimental temperature range down to 2600K where the evaporation rates are the lowest. We conclude from this result that the process of laser-based evaporation is in fact transport limited under the conditions used in this study and that h_m and K_p are the rate controlling parameters for the process. The apparent transport limitations with pure nitrogen further indicates that it is the transport of the products out of the boundary layer that is limiting the *R* since no gas phase reactants are present in pure nitrogen and air [8].

3.2 Evaporation kinetics

Having established the dependence of *R* on mass transport kinetics, which suggests that the process is near-equilibrium, the dependence of silica evaporation on the gas chemistry was determined from measurements of the *R* in the presence of air, pure nitrogen, 5% hydrogen in nitrogen, and 5% hydrogen in helium. Figure 3 shows a strong dependence of *R* on the type of gas used. The reduction of silica by hydrogen produced greater evaporation rates than evaporation in an inert nitrogen atmosphere, and pure nitrogen produced greater rates than evaporation in air, an oxidizing environment. Hydrogen effectively reduced silica vapor pressure by about 100-200K compared to ambient conditions. These results were not unexpected since the main endothermic reactions thought to occur at the experimental temperatures are as follows [8]:

$$SiO_2(l) \Leftrightarrow SiO(g) + \tfrac{1}{2}O_2(g) \qquad (1)$$

$$SiO_2(l) + H_2(g) \Leftrightarrow SiO(g) + H_2O(g) \qquad (2)$$

With the realization that these reactions are driving the evaporation, interpretation of the results in Fig. 3 become straightforward. Reaction (1) is the main decomposition reaction in the presence of all gases used. The secondary reaction (2) occurs only when hydrogen is added in the gas mixture, providing an additional pathway for the evaporation of silica, which is confirmed by the increased *R* in the presence of hydrogen in Fig. 3. The presence of O_2 manifests itself in two ways. First, evaporation in air is lowered compared to pure nitrogen due to the presence of O_2. Second, the O_2 evolved in reaction (1), which increases at higher temperatures, tends to slow evaporation by shifting the equilibrium of reaction (1) backward. This shift is apparent in the pure nitrogen and hydrogen data above T~2900K where *R* becomes sub-linear, as indicated by the arrows in Fig. 3. The shift is less apparent in air because of the already elevated amount of O_2 (21%) present. Thus, in air, the O_2 produced in reaction (1) does not alter its concentration significantly as indicated by the linearity of *R* up to the highest temperatures in Fig. 3. For comparison, the maximum evaporation rates were predicted from the Hertz-Knudsen equation, $R=P_{sat}(T)/\sqrt{2\pi m k_B T}$, where P_{sat} is the vapor pressure of SiO in reaction (1) [8], m is the molecular mass, and k_B is the Boltzmann constant. Not surprisingly, the rates predicted are orders of magnitude greater (Fig. 3) because the Hertz-Knudsen model does not account *a priori* for the mass

transport limitations that prevails in this laser-based evaporation study. Also, the contrasting temperature dependence and slope in Fig. 3 reflect the fact that the Hertz-Knudsen formula is derived from the kinetic theory of gases, which scales the escape velocities as $1/\sqrt{T}$, while the temperature dependence of the near-equilibrium described below depends on the thermodynamics of the evaporation process and, to a lesser extent, on the temperature dependence of the transport kinetics.

The mass transport problem was further addressed in a separate experiment carried out in helium instead of nitrogen as the carrier gas but with the same hydrogen fraction. The magnitude of R in helium was expected to be larger because the gas phase diffusivity in helium is larger than in nitrogen [16, 31, 32], which should result in a greater h_m and R in helium if mass transport is the limiting transport mechanism. An increase in R is indeed observed in Fig. 3, which validates our initial assessment from Fig. 2 that the process of laser-based evaporation in our system is mass transport limited. In the transport limited regime, the molar evaporation rate can then be approximated as a function of the h_m and the equilibrium SiO concentration, $[SiO]_{eq}$. Thus, given a product-free gas feed [24],

$$R \sim h_m \times [SiO]_{eq} \qquad \textbf{(3)}$$

It is on the basis of equation (3) that the remainder of the analysis of R will be performed, first, by focusing on calculating the equilibrium case and, second, by determining the h_m for our experiments as discussed below.

3.3 Calculation of the reaction thermodynamics

Although the evaporation data in Fig. 3 could be interpreted on the basis of chemical equilibria and transport, a quantitative approach involves the calculation of the equilibrium species concentration based on the temperature dependent K_p. K_p is given by the free energy, $\Delta G^\circ=\Delta H^\circ-T\Delta S^\circ$, of reaction (1) and (2): $K_p = \exp(-\Delta G^\circ/R_cT)$, where R_c is the gas constant and T the temperature. A system of coupled equations can then be derived by treating the overall reaction (1) and (2) as elementary reactions:

$$\left(\frac{n_{i-SiO}+\xi+\alpha}{n_T}\right)\left(\frac{n_{i-O2}+1/2\xi}{n_T}\right)^{0.5}P^{3/2}=K_{p1}(T) \qquad (4)$$

$$\left(\frac{n_{i-H2}-\alpha}{n_T}\right)^{-1}\left(\frac{n_{i-SiO}+\alpha+\xi}{n_T}\right)\left(\frac{n_{i-H2O}+\alpha}{n_T}\right)P=K_{p2}(T) \qquad (5)$$

The terms in parenthesis represent mole fractions, P is the total pressure taken as 1 atm in our system, n_i are the initial species quantity in moles, α and ξ, are the extent of reaction for each reaction, n_T represents the total number of moles calculated based on the n_i and α and ξ. Standard free energies, ΔG°, are available in the literature [8] and in thermodynamic databases [33].

In order to compare the equilibrium concentrations calculated from (4)-(5) with the evaporation data in Fig. 3, the data is re-plotted in Fig. 4A as the ratio of the R in each gas. This approach allows us to decouple the mass transport from the thermodynamic problem, such that from equation (3): $R(N_2)/R(\text{air})\sim[SiO]_{eq}(N_2)/[SiO]_{eq}(\text{air})$. In this way, the data in Fig. 4A can be compared directly to the calculated equilibrium concentrations or, equivalently, mole fractions. The implied approximation that $h_m(\text{air})\sim h_m(N_2)$ is reasonable because the gases selected have nitrogen as their main constituent ranging from 80 to 100% N_2, thus the transport properties of the gas mixtures are expected to be similar. Figure 4A shows a comparison of the experimental ratio of R for evaporation in nitrogen relative to air with the two curves representing the ratio calculated from (4) and the ΔG° for reaction (1) reported from two sources [8, 33]. The corresponding calculated equilibrium SiO mole fractions are provided in Fig. 4B. Although the predictions agree with the data at higher temperatures, at lower temperatures a discrepancy is apparent even when accounting for the gap between the two predictions. However, since the discrepancy is within the spread in the data, and the reported ΔG° represent an extrapolation from data below about 2000K, the ΔG° for reaction (1) was fitted to extract an effective ΔG° (Fig. 4). The resulting enthalpy, entropy, and free energy of reaction are summarized in Table 1, along with the fitted empirical Arrhenius parameters added for reference.

The sources of the discrepancy are uncertain, and comparison of ΔG° from data in this study below 2000 K are not possible because evaporation rates are too slow to be measured as discussed in section 2.1. For evaporation in pure nitrogen relative to that in air, the data under-predicts the ratio $R_{N2}(T)/R_{air}(T)$ compared to that calculated based on the reported free energies. In other words, the experimental

evaporation rates in air and nitrogen are closer than expected. The temperature dependence of the discrepancy is difficult to explain on the basis of, for example, concentration dependent diffusivity, on the non-isothermal conditions related to the Gaussian laser beam heating, or on the possibility of re-deposit material affecting the measured pit depth. However, evaporation rates and the resulting mass transfer limitations become greater at higher temperatures; these are also conditions that more closely approximate a local equilibrium. Therefore it is reasonable to expect that the near-equilibrium-based model represented by (3)-(5) should result in better agreement at higher temperatures (Fig. 4A).

With the hydrogen gas mixture, a discrepancy in the experimental versus calculated ratios of R (H_2 mixture/pure N_2) was also observed (Fig. 5A). Again, the data was fitted to extract an effective $\Delta G^\circ$for reaction (2) (Table 1) for the temperatures reached between 2600 K and 3000 K. However, this time, unless a fixed hydrogen concentration was used when solving (4)-(5), the data could never be fitted irrespective of the ΔG° value. This point is illustrated in Fig. 5B, where the dashed curve representing the calculated ratio with an "initial" 5% hydrogen mixture, remains persistently below the data points. With this initial 5% hydrogen fraction, the calculated hydrogen concentration equilibrates locally to values between 0.5% and 2.5% for temperatures ranging from 2600K to 3000K, respectively. In contrast, with a "fixed", invariant 5% hydrogen concentration, the data can now be readily fitted since the predicted ratio based on the reported ΔG° remains below experimental results. The ΔG° values used to plot the experimental ratio were determined from the enthalpy and entropy in Table 1 and the measured temperatures. The need to keep the hydrogen fixed in order to fit the data suggests that the mass transport of hydrogen is fast enough to maintain a bulk hydrogen concentration throughout the gas-solid interface where it is being consumed in reaction (2). This insight is consistent with the previous observation (section 3.1) that the transport of the products, and not the reactants, is rate limiting. Thus a fixed 5% hydrogen concentration, along with the derived ΔG° (Table 1) were used to complete the modeling of R and to calculate the predicted ratio. In contrast with the $R_{N2}(T)/R_{air}(T)$ ratio in Fig. 4, the 5% $R_{H2}(T)/R_{N2}(T)$ data over-estimate the prediction although, once again, the agreement improves at higher temperature where the conditions for near-equilibrium are more closely approximated as in the air/nitrogen case. This over-estimate indicates that the evaporation rates in 5% hydrogen and pure nitrogen are further apart than expected. A potential explanation is that the current model does not account for the possibility that hydrogen may also be reacting with the oxygen evolving from reaction (1), thereby pushing the reaction forward to produce greater than expected evaporation rates. Hydrogen could thus react both with silica directly (reaction (2)) and with oxygen to form water vapor ($H_2(g) + ½O(g) \Leftrightarrow H_2O(g)$) . Reaction (1) would also take place simultaneously. We are currently addressing this scenario analytically and experimentally for future publication.

3.4 Calculation of the transport kinetics

The analysis above was based on the relative R in each gas. A complete expression of the absolute R requires the determination of not only the equilibrium SiO concentrations (section 3.1), but also of the mass transport kinetics expressed in the h_m. Although many semi-empirical correlations can be used to determine h_m in the laminar or turbulent regime [34, 35], none were found for the nozzle- impinging flow configuration in our experimental setup. Therefore the h_m must be extracted from our data by

fitting across the two variables on which it depends: temperature and flow rate. *R* data in Fig. 2 and 3 were fitted for h_m using equation (3) written more explicitly now as $R(T,V)=h_m(T,V)\times[SiO]_{eq}(T)$, where *V* is the gas feed volumetric flow rate and the $[SiO]_{eq}(T)$ is determined for each gas from the fitted reaction free energies in section 3.1. For this purpose, generalized expressions describing the kinetics of transport using a boundary layer approximation are useful. Typically used are the dimensionless Sherwood number, *Sh*, which relates *Sh* to the Reynolds, *Re*, and the Schmidt number, *Sc*. *Sh* is defined such that $Sh = h_mL/D = f(Sc=\mu/\rho D, Re=\rho VL/\mu)$, where *L* is a characteristic length (taken as the beam diameter), μ the dynamic viscosity, *D* the species diffusivity, and ρ the gas density. All the temperature dependent gas properties in the model were calculated from available data and empirical models to extrapolate the viscosity [36], diffusivity [31], and from the ideal gas law for density. To simplify the problem, all the gas mixtures were treated as pure nitrogen, since this is the dominant species. The particular form of the empirical expression for h_m is given by:

$$Sh = C\,Sc^m\,Re^n \qquad (6)$$

where *C*, *m*, and *n* represent a single set of fitting parameters applicable for all the gases used in this study. As shown in Fig. 3 this expression provides a good fit to the data with the corresponding *C*, *m*, and *n* given in Table 1.

Conclusions

With h_m determined and the equilibrium concentration calculated from K_p, a predictive model for the laser-based evaporation of silica is now available which accounts for the temperature dependent gas properties, the thermodynamics of the reaction of the gas phase reactant, and the mass transport configuration in the flow system. The experimental method, along with the analysis should be applicable to a broad range of materials exposed to both steady state heating with lasers and to gases with selected reactivities. The critical insight of this study is that the process is mass-transport limited and therefore dependent on the thermodynamics of the reactions through the free energy. The present analysis can also form the basis to interpret evaporation rate data at extreme temperatures, typically only reachable with laser heating. Thus, this approach could potentially enable the derivation of thermodynamic properties of gas-solid phase reactions at extremes temperatures, provided that accurate measurement of the evaporation rates and temperatures are made. The approach can also provide insights into the mechanism by which specific gases interact with the solid during reactive etching and should improve control of thermal etching processes in general.

Acknowledgements

The authors would like to thank Dr. Michael Feit for useful discussions on silica evaporation chemistry, and Sherry Baker for her assistance with white-light interferometry measurements. This work performed under the auspices of the U.S. Department of Energy by Lawrence Livermore National Laboratory under Contract DE-AC52-07NA27344.

Table 1

Effective entropy and enthalpy values derived from fitting of the temperature dependent evaporation rate data obtained between 2600 K and 3000 K for laser heated silica. The corresponding experimental reaction free energies are calculated from $\Delta G^\circ = \Delta H^\circ - T\Delta S^\circ$ and compared to reported ΔG° values from Ref(33) in parenthesis. Likewise, fitting parameters for the mass transfer coefficient of the SiO evaporation product, h_m, were derived from the measured evaporation rates in air, pure nitrogen, and in a 5% hydrogen-95% nitrogen gas mixture. The evaporation rate data in Fig. 3 were fitted to yield an apparent activation energy, E_a, and a pre-exponential A_m in the Arrhenius relation, $R(T)=A_m\exp(-E_a/RT)$ for each gas used in this study.

	ΔH° (kcal/mol)	**ΔS° (cal/mol.K)**	**ΔG°(3000 K) (kcal/mol)**
$SiO_2 \Leftrightarrow SiO + ½O_2$	62.3	15.9	14.6 (15.5)
$SiO_2 + H_2 \Leftrightarrow SiO + H_2O$	68.5	24.6	-5.4 (-3.0)
h_m	$C = 1.42\times10^{-17}$, n = 0.1, m = -2.5		
Arrhenius fitting parameters	***E_a* (kcal/mol)**		***A_m* (μg/μm^2.sec)**
air(dry)	120.1		6.25×10^{3}
100% nitrogen	101.3		3.18×10^{2}
5% hydrogen, 95% nitrogen	110.9		3.14×10^{3}

FIGURES

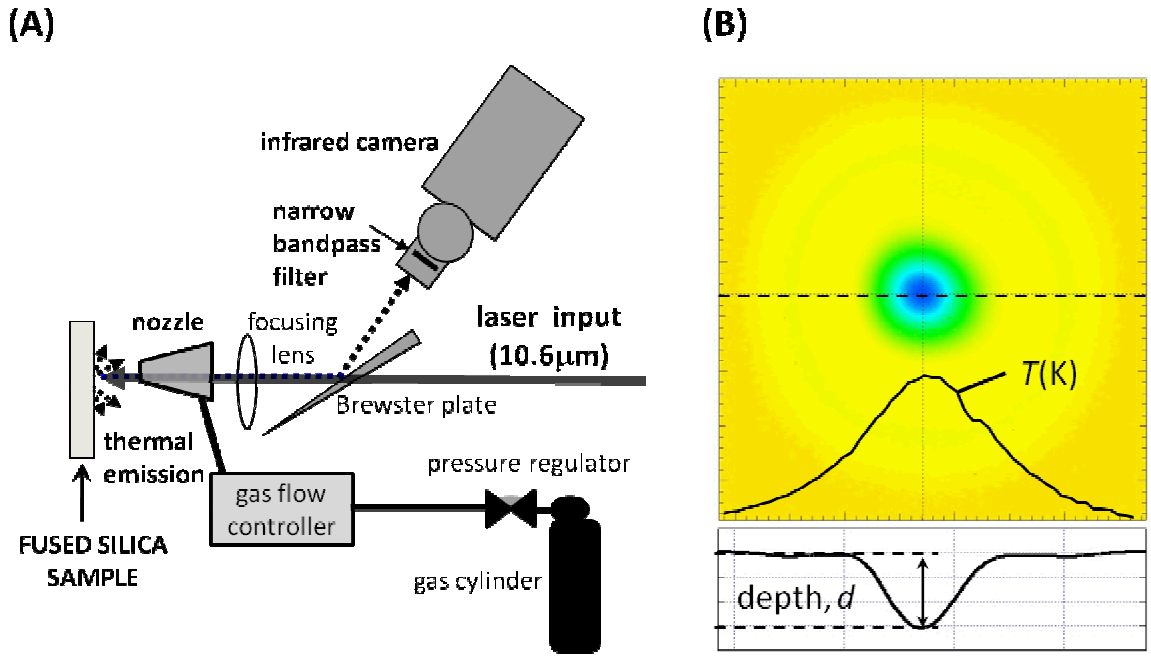

Figure 1. (A) Schematic of the experimental setup used for evaporation of fused silica with CO_2 laser heating. A nozzle is used to bring an impinging gas coincidently with the laser beam at a controlled flow rate of the treatment gas. (B) The laser-based evaporation produces a pit for which the surface profile is measured using white light interferometry. The surface depth profile is shown for the line-out drawn through the center of the pit, along with the corresponding surface temperature profile, *T*(K), captured *in situ* with an infrared camera and the bottom pit depth, *d*.

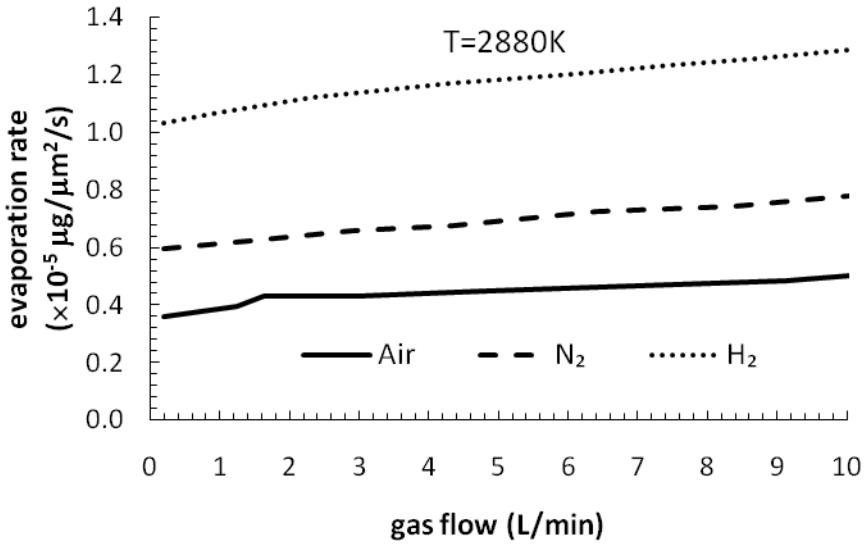

Figure 2. Measurements of the evaporation rate dependence on the gas feed volumetric flow rate for *T*=2880 K.

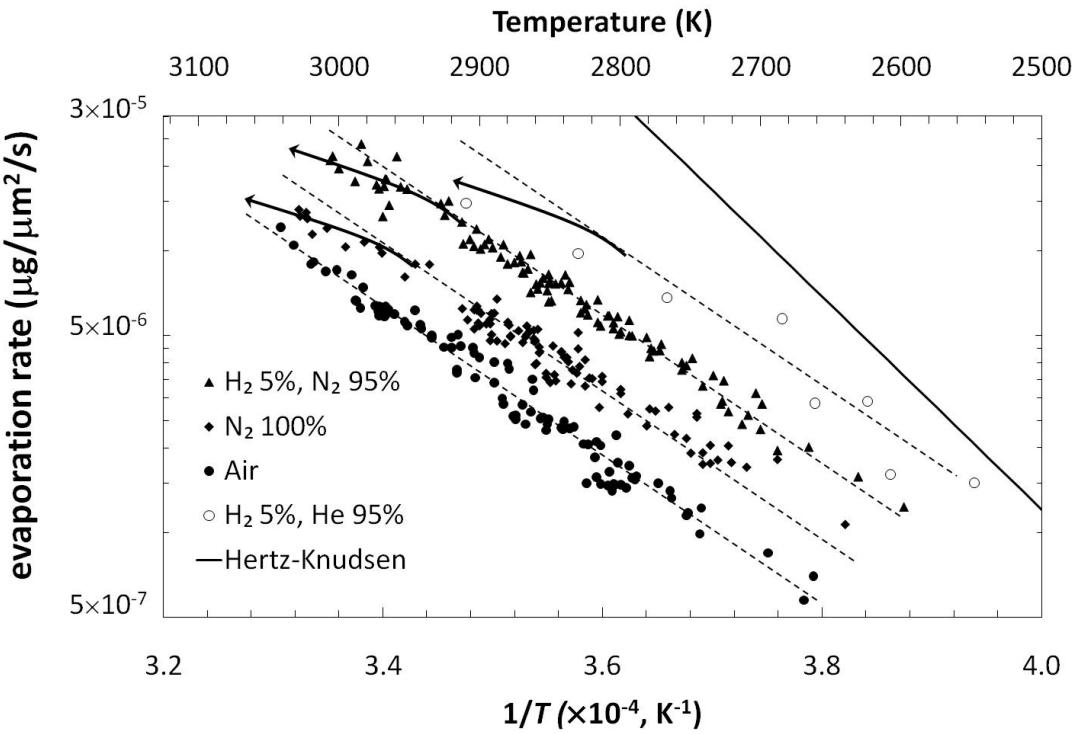

Figure 3. Measurements of the temperature dependent fused silica evaporation rates for the gases indicated. Dashed lines and arrows are used to guide the eye. The solid line represents the estimated evaporation rates from the Hertz-Knudsen equation based on the reported vapor pressures of SiO in Ref(8) and an evaporation coefficient of one. The values from the H-K model are scaled by a factor of ×1/30 for clarity.

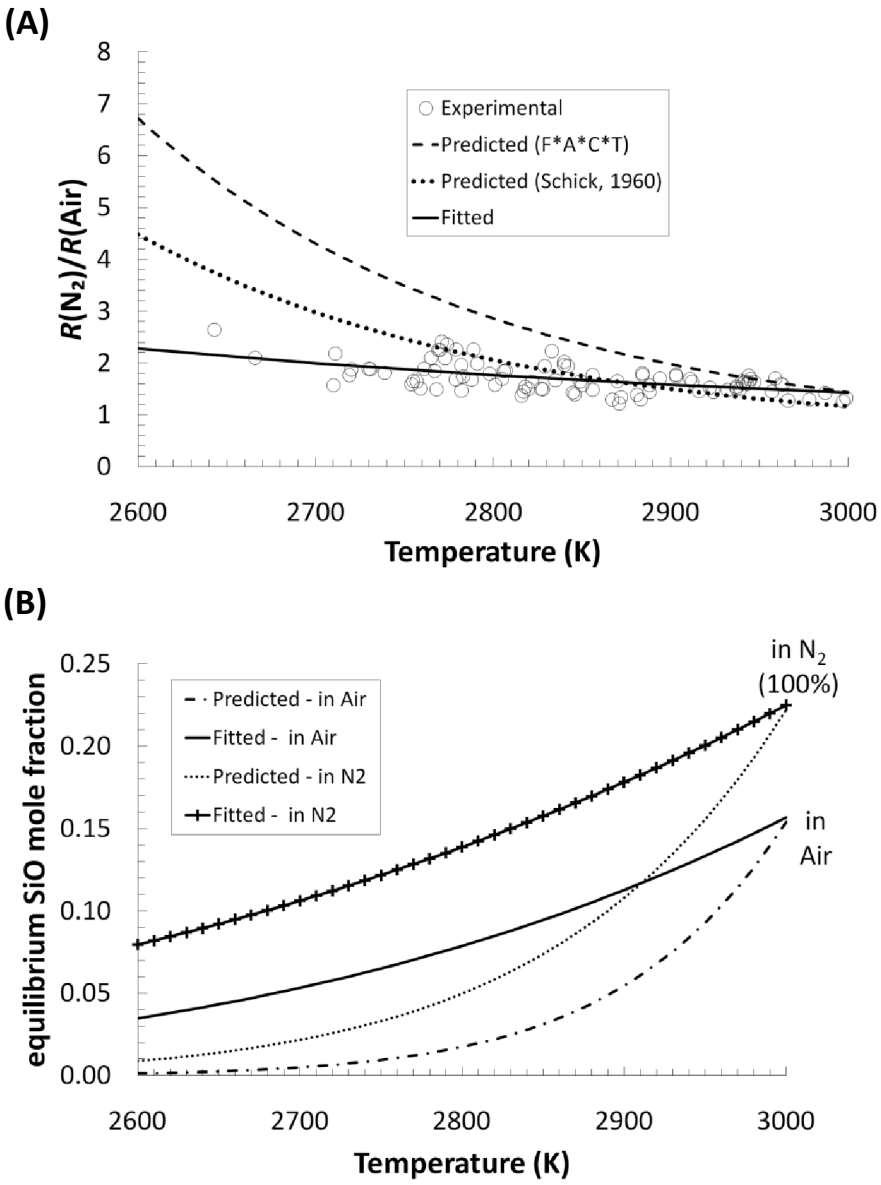

Figure 4. (A) Experimental evaporation rates for the thermal decomposition of fused silica in pure N_2 relative to evaporation in air. Relative evaporation rates were also calculated based on reported values ΔG° for reaction (1) from the sources indicated in Ref(33) and Ref(8). The data was fitted (solid line) to extract an effective temperature-dependent ΔG° for reaction (1). (B) The corresponding predicted molar fractions of SiO product are shown for each gas using ΔG° reported in Ref(33) (dashed lines), and compared to those based on a ΔG° obtained in the fitting in (a) (solid lines).

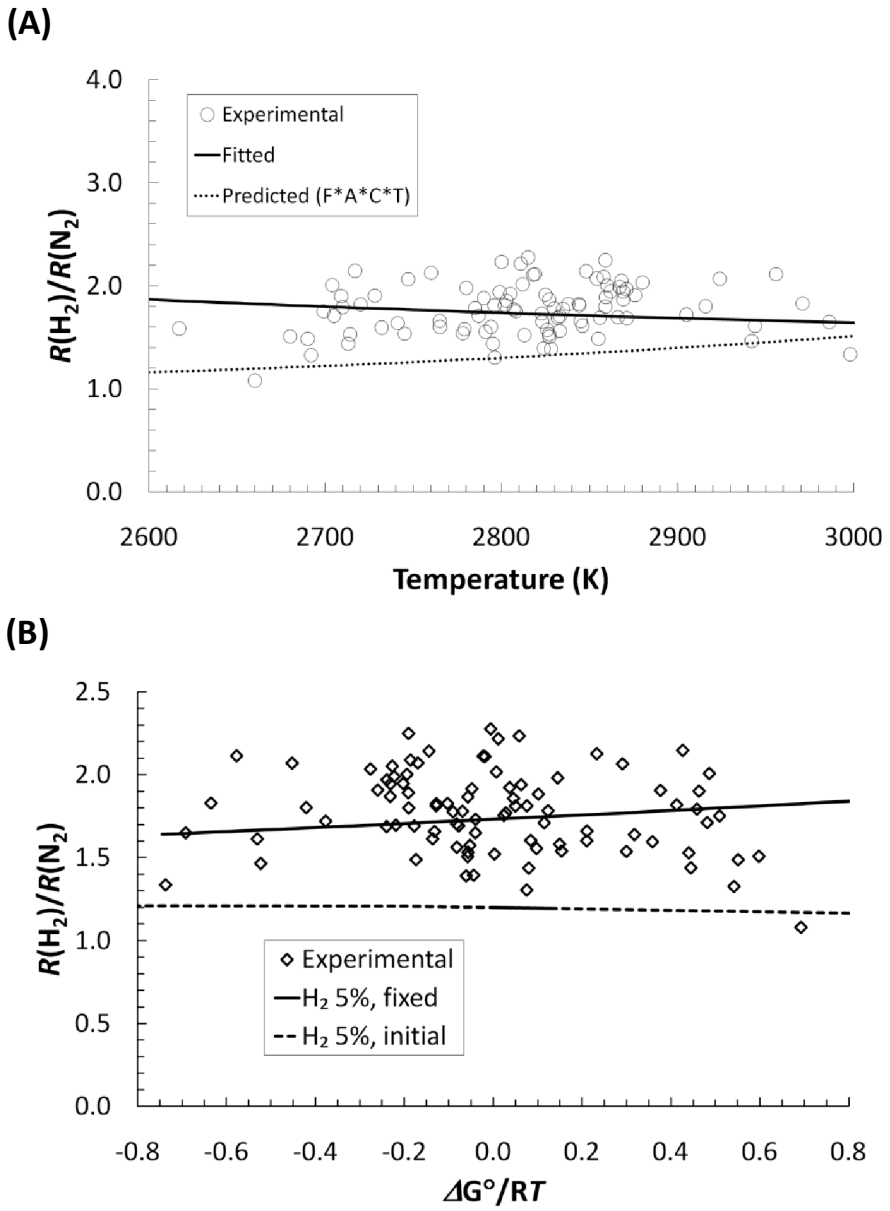

Figure 5. (A) Experimental evaporation rates in 5% H_2, 95% N_2 gas relative to evaporation in pure N_2 ($R(H_2)/R(N_2)$). Relative evaporation rates were also calculated based on reported $\Delta G°$ values for reaction (2) from Ref(33) database. The data was fitted to extract an effective temperature-dependent $\Delta G°$ for reaction (2) from which the $R(H_2)/R(N_2)$ ratio could be plotted (solid line). (B) The experimental $R(H_2)/R(N_2)$ in (A) are compared to the calculated ratio based on a range of $\Delta G°/RT$ values for an initial H_2 concentration of 5% (dashed line) and for a fixed 5% H_2 concentration.

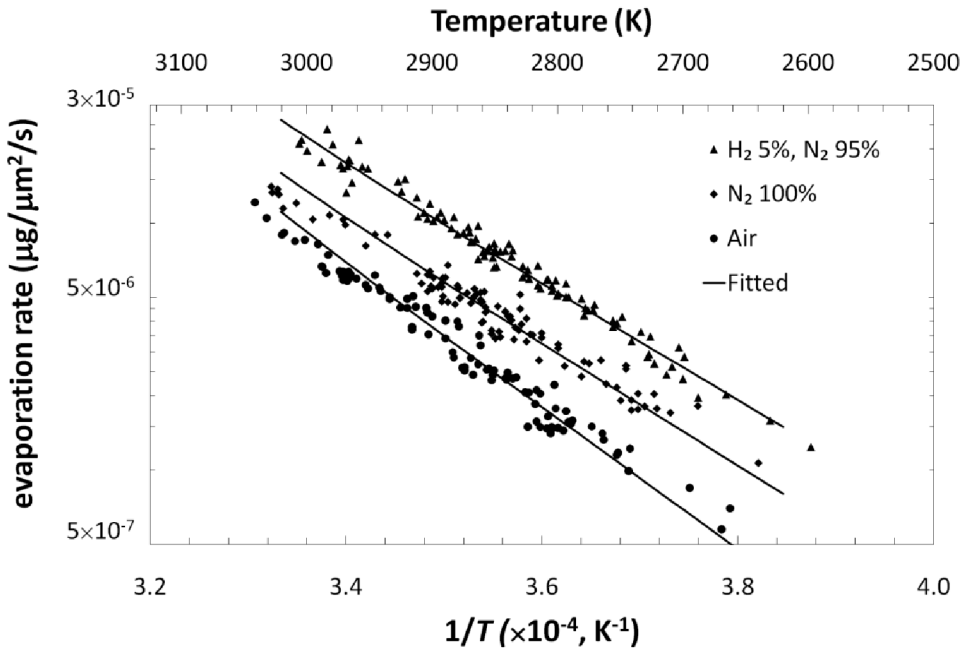

Figure 6. Experimental evaporation rates in the indicated gases were used to extract the mass transfer coefficient parameters from the fitted data (solid lines).

REFERENCES

[1] M.T. Lee, Journal of the American Ceramic Society, 67 (1984) C21.
[2] G. Montano-Miranda, A. Muscat, Ultra Clean Processing of Semiconductor Surfaces Viii, 134 (2008) 3.
[3] J.F. Bacon, A.A. Hasapis, J.W. Wholley, Physics and Chemistry of Glasses, 1 (1960).
[4] R. Brückner, Journal of Non-Crystalline Solids 5(1970) 123.
[5] J.F. Shackelford, P.L. Studt, R.M. Fulrath, Journal of Applied Physics, 43 (1972) 1619.
[6] R.H. Doremus, Journal of Applied Physics, 92 (2002) 7619.
[7] S.T. Yang, M.J. Matthews, S. Elhadj, D. Cooke, G.M. Guss, V.G. Draggoo, P.J. Wegner, Applied Optics, 49 (2010) 2606.
[8] H.L. Schick, Chemical Reviews, 60 (1960) 331.
[9] I.L. Bass, G.M. Guss, M.J. Nostrand, P.J. Wegner, An Improved Method of Mitigating Laser Induced Surface Damage Growth in Fused Silica Using a Rastered, Pulsed CO2 Laser, in: Laser-Induced Damage in Optical Materials: 2010, Proceedings of SPIE-The International Society for Optics and Photonics, Boulder, CO, USA, 2010, pp. 784220.
[10] E. Mendez, K.M. Nowak, H.J. Baker, F.J. Villarreal, D.R. Hall, Applied Optics, 45 (2006) 5358.
[11] V.K. Sysoev, V.I. Masychev, B.P. Papchenko, S.Y. Rusanov, A.A. Yakovlev, N.P. Glukhoedov, Inorganic Materials, 39 (2003) 532.
[12] P. Cormont, L. Gallais, L. Lamaignere, T. Donval, J.L. Rullier, Effect of CO2 laser annealing on residual stress and on laser damage resistance for fused silica optics, in: Laser-Induced Damage in Optical Materials: 2010, Proceedings of SPIE-The International Society for Optics and Photonics, Boulder, CO, USA, 2010, pp. 78422C.
[13] M.J. Matthews, I.L. Bass, G.M. Guss, C.C. Widmayer, F.L. Ravizza, Downstream intensification effects associated with CO2 laser mitigation of fused silica - art. no. 67200A, in: Laser-Induced Damage in Optical Materials: 2007, Proceedings of SPIE-The International Society for Optics and Photonics, Boulder, CO, USA, 2007, pp. 67200A.
[14] D.M. Mattox, H.D. Smith, Journal of the American Ceramic Society, 71 (1988) C392.
[15] S.T. Tso, J.A. Pask, Journal of the American Ceramic Society, 65 (1982) 457.
[16] K. Schwerdtfeger, Transactions of the Metallurgical Society of Aime, 236 (1966) 1152.
[17] R.A. Gardner, Journal of Solid State Chemistry, 9 (1974) 336.
[18] J. Stone, Journal of Lightwave Technology, 5 (1987) 712.
[19] T. Addona, R.J. Munz, Industrial & Engineering Chemistry Research, 38 (1999) 2299.
[20] J.F. Shackelford, J.S. Masaryk, Journal of Non-Crystalline Solids, 21 (1976) 55.
[21] A. de Rudnay, Vacuum, 1 (1951) 204.
[22] L. Pekker, N. Gimelshein, S. Gimelshein, Journal of Thermophysics and Heat Transfer, 23 (2009) 473.
[23] G. Han, H.Y. Sohn, Journal of the American Ceramic Society, 88 (2005) 882.
[24] H.Y. Sohn, Metallurgical and Materials Transactions B-Process Metallurgy and Materials Processing Science, 35 (2004) 121.
[25] S.T. Yang, M.J. Matthews, S. Elhadj, V.G. Draggoo, S.E. Bisson, Journal of Applied Physics, 106 (2009) 103106.
[26] S. Elhadj, M.J. Matthews, S.T. Yang, D.J. Cooke, J.D. Bude, M. Johnson, M. Feit, V. Draggoo, S.E. Bisson, High temperature thermographic measurements of laser heated silica, in: G.J. Exarhos, V.E. Gruzdev, D. Ristau, M.J. Soileau, C.J. Stolz (Eds.) Laser-Induced Damage in Optical Materials: 2009 Proceedings, Proceedings of SPIE-The International Society for Optics and Photonics, Boulder, CO, 2009, 2009, pp. 750419.
[27] S. Elhadj, M.J. Matthews, S.T. Yang, D.J. Cooke, J.S. Stolken, R.M. Vignes, V.G. Draggoo, S.E. Bisson, Applied Physics Letters, 96 (2010).

[28] N.M. Bulgakova, A.V. Bulgakov, Applied Physics a-Materials Science & Processing, 73 (2001) 199.
[29] T.J. Mcneil, R. Cole, R.S. Subramanian, Journal of the American Ceramic Society, 68 (1985) 254.
[30] A. Kar, J. Mazumder, Journal of Applied Physics, 68 (1990) 3884.
[31] W.J. Massman, Atmospheric Environment, 32 (1998) 1111.
[32] B. Ozturk, R.J. Fruehan, Metallurgical Transactions B-Process Metallurgy, 16 (1985) 801.
[33] F*A*C*T, in, 2010, pp. Facility for the Analysis of Chemical Thermodynamics.
[34] S.W. Churchill, H.H.S. Chu, International Journal of Heat and Mass Transfer, 18 (1975) 1323.
[35] S.W. Churchill, H.H.S. Chu, International Journal of Heat and Mass Transfer, 18 (1975) 1049.
[36] CRC Handbook of Chemistry and Physics, 65th ed., CRC Press, Boca Raton, FL, USA, 1984.

Supplementary Information

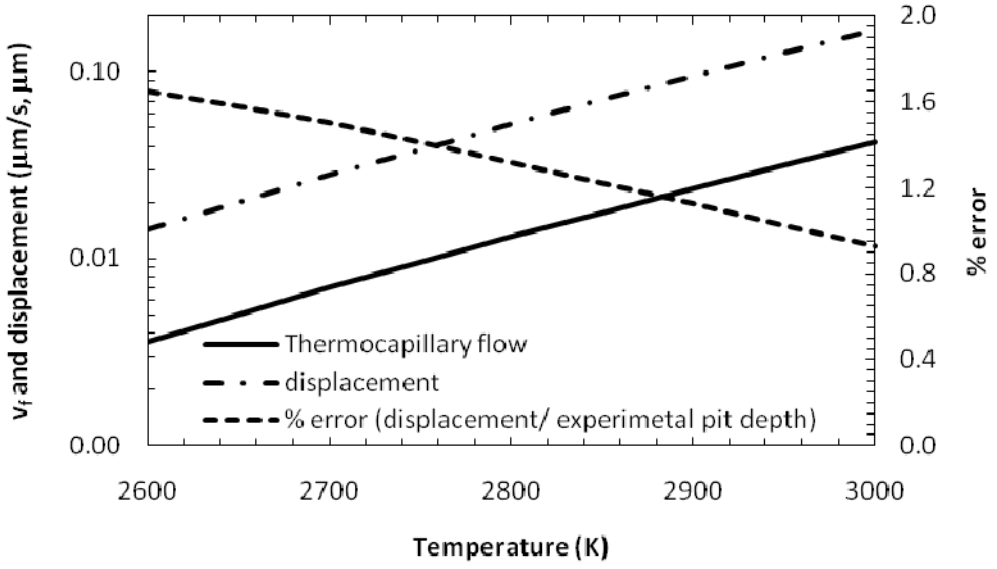

Figure 1S. Estimates of thermocapillary flow velocities arising from surface tension gradient in silica during laser heating, $v_f = |d\gamma/dT| \Delta T/\mu$. The surface displacement is then given by $v_f \times \Delta t$, where Δt is the laser exposure time. The temperature drop, ΔT, is based on the difference between the peak temperature, T_p, at the center of the pit and T_g~1673 K near the melted edge of the pit. The kinetic viscosity, μ, was determined from the relation $\mu = \mu_0 \exp(E_a/RT)$, where $\mu_0 = 3\times10^{-9}$ Poise, E_a=603 kJ/mol (Shen *et al*, "Laser smoothing of sub-micron grooves in hydroxyl-rich fused silica", *Appl. Surf. Sc.*, 256, pp4031-4037), and the temperature, T, of the heated molten layer is taken as the arithmetic average = $(T_p+T_g)/2$. $d\gamma/dT = -1.4\times10^{-4}$ N/m.K is the rate of change of the surface tension with temperature taken from Parikh *et al*, "Effect of atmosphere on surface tension of glass", *J. Am. Cer. Soc.*, 41(1), pp18-22.